Using SEMM to Identify the Joint Dynamics in Multiple Degrees of Freedom Without Measuring Interfaces.

S. W. B. Klaassen, D. J. Rixen

Technische Universität München, Boltzmannstr. 15, 85748 Garching, Germany

ABSTRACT

As the number of models created in a modular fashion increase, the need for accurate identification of real joint dynamics rises. Since joint dynamics are a consequence of component-to-component interaction, they are only present in the assembled state. Yet, it is in the assembled state that measuring the interface degrees of freedom is practically infeasible. Nevertheless, the effects of the joint are present in measurements throughout the component, i.e. the joint dynamics are observable. In this work, system equivalent model mixing is used to expand an experimental measurement with interface degrees of freedom –either rotational or translational– extracted from a numerical model. Subsequently, joint dynamics can be obtained by applying classic frequency based decoupling methods. The strength of this method lies in the ability to test different interface configurations from a single measurement campaign, limited only by the the actual number of sensor or impact locations. The paper shows that an updating scheme can be used to identify joint dynamics without directly measuring interfaces.

Keywords: System Equivalent Model Mixing, Interfaces, Joint identification, Optimization.

1 INTRODUCTION

While the influence of joints is not always prevalent, they are one of a structure's main sources of uncertainty and unreproducibility. This is in part due to the lack of understanding of joint mechanisms which essentially result in *unidentified* dynamic influence. Although joints are often mistreated as an unfortunate consequences of today's assembly-based manufacturing, they are sometimes beneficial and in fact necessary: e.g. In turbine systems, the damping caused by friction contacts may help reduce the resonance amplitudes (which allows for smaller gaps between turbine blades and casing) and reduces the possibility of instability [1]. Identifying different joints will advance the understanding of joint mechanisms, which in turn allows us to steer towards these beneficial joint effects, rather than the unfavourable uncertainty.

In order to identify the joint, it must be observed. This is classically done by measuring physical effects or dynamic responses at the interfaces of the assembled system. Yet, in this assembled state it is highly impractical to perform measurements directly at, or even near the joint. To work around this problem a simplification is often introduced; common examples of such simplifications are reducing the DoF of the joint to a number and direction that can be measured, or by extrapolating the effects observed in the measurable areas (such as the sides of the assembly) over the total (unmeasurable) area of the interface.

Fortunately, the dynamic effect of the joint is observed in other responses (not on the interface) combined with the effects of the sub-components themselves. Therefore, if the effects of the components are removed, one can single out the joint dynamics. In [2, 3], joint identification is done by assuming a two-DoF joint[1] at the interface and using substructure decoupling to remove the effects of the known components from the assembled system. Even so, information is needed at the joint itself which requires impact locations and sensors to be placed there, referring back to the problem stated above.

[1] The deflection and rotation in a beam.

If, however, the DoF at the interface are not measured but calculated by means of an expansion method, these limitations no longer hold. System Equivalent Model Mixing (SEMM) is a method based on frequency based substructuring that can be used to expand a measurement's DoF-set by coupling the measurement-based model to an equivalent –yet not identical– model with the required boundary DoF [4]. Note that this model only needs to have the required DoF, and not the correct joint dynamics (since these are provided by the measurement).

Outline of the paper

In this work, SEMM is used to expand the DoF-set of assembled-system measurements to include the boundary DoF required to identify the joint. In section 2 the theory will be explained: The theory starts with section 2.1 which covers the Lagrange Multiplier Frequency Based Substructuring (LM-FBS) method, including weakly-formulated interface problems in order to lay-down the basis for SEMM as well as explain the additional steps required to perform joint identification. Once LM-FBS is covered, the SEMM method will be highlighted in section 2.2. In section 2.3, an optimisation scheme is introduced which deals with the inherent errors of SEMM expansion.

A proof of concept is given in section 3 where a simple numerical case is presented to showcase the abilities and limitations of the method. Finally, in section 4 and 5, a critical discussion and conclusion are provided alongside a prognosis for work induced by this concept.

2 THE JOINT IDENTIFICATION METHOD

A multitude of joint-types exist and thus the term is used broadly. For the context of this paper however, a joint is simply a cause of additional dynamics which exists only when two substructures are coupled. Therefore, where others would differentiate between bolts, welds, adhesives, contact-friction, etc. in this work a joint encompasses all. This is because the method discussed in this paper assumes that the *joint* is a black-box, and by removing the *known* component dynamics from the system dynamics this black-box is identified. It is important to note that the linearity assumption of the frequency based methods applies to the joint as well, and thus only linear (or linearised) properties of the joint can be identified.

Additionally, an important distinction is made between the joint and the interface. A joint is an actual source of dynamics whereas the interfaces are the sets of degrees of freedom on each side of the sub-component between which the joint acts. For example, in Figure 1 a schematic of a standard (read: rigid) coupling problem is depicted. The interfaces are described by the red markers and the joint (in this case a rigid link) acts between the interfaces.

2.1 Frequency Based Substructuring: Coupling and Decoupling with a weak-formulated joint

Frequency based substructuring (FBS), or more specifically Lagrange Multiplier Frequency Based Substructuring (LM-FBS) is a dual-method that operates in the frequency domain and in admittance space; it therefore allows the user to directly implement measured Frequency Response Functions (FRF) [5]. Considering that performing measurements is the only way to identify the *unknown* joint dynamics, it is advantageous to use methods that agree with *measurement data*, i.e. FRF.

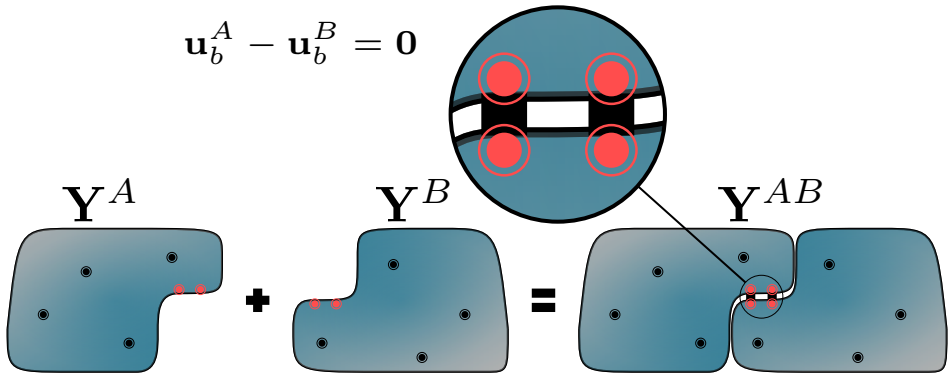

Figure 1: Component A is connected to component B via a rigid connection. The black markers represent the internal DoF $\mathbf{u}_i$ and the red markers represent the boundary DoF $\mathbf{u}_b$. Due to the rigid connection the compatibility condition states that $\mathbf{u}_b^{\mathrm{A}} - \mathbf{u}_b^{\mathrm{B}} = \mathbf{0}$.

The equation of motion in the frequency domain for a general dynamic component s is given as follows:

$$\mathbf{u}^s(\omega) = \mathbf{Y}^s(\omega)\left(\mathbf{f}^s(\omega) + \mathbf{g}^s(\omega)\right) \tag{1}$$

where $\mathbf{u}^s(\omega)$ are the responses to the (known) external forces $\mathbf{f}^s(\omega)$ and (unknown) internal forces $\mathbf{g}^s(\omega)$ through the admittance matrix $\mathbf{Y}^s(\omega)$. In figure 1, components A and B are shown, their equations of motion can be derived in the form of equation (1). The implicit dependency on the frequency ω is omitted here for clarity, and will be done so for the remainder of the paper.

$$\mathbf{u}^{\mathrm{A}} = \mathbf{Y}^{\mathrm{A}}\left(\mathbf{f}^{\mathrm{A}} + \mathbf{g}^{\mathrm{A}}\right) \tag{2}$$
$$\mathbf{u}^{\mathrm{B}} = \mathbf{Y}^{\mathrm{B}}\left(\mathbf{f}^{\mathrm{B}} + \mathbf{g}^{\mathrm{B}}\right) \tag{3}$$

These can then be combined into block-form:

$$\mathbf{u} = \mathbf{Y}\left(\mathbf{f} + \mathbf{g}\right) \quad \text{where:} \quad \mathbf{Y} = \begin{bmatrix} \mathbf{Y}^{\mathrm{A}} & \\ & \mathbf{Y}^{\mathrm{B}} \end{bmatrix}, \quad \mathbf{u} = \begin{bmatrix} \mathbf{u}^{\mathrm{A}} \\ \mathbf{u}^{\mathrm{B}} \end{bmatrix}, \quad \mathbf{f} = \begin{bmatrix} \mathbf{f}^{\mathrm{A}} \\ \mathbf{f}^{\mathrm{B}} \end{bmatrix}, \quad \mathbf{g} = \begin{bmatrix} \mathbf{g}^{\mathrm{A}} \\ \mathbf{g}^{\mathrm{B}} \end{bmatrix} \tag{4}$$

The models are coupled via the internal forces $\mathbf{g}$ which act only on the boundary DoF (c.f. the red markers in Figure 1), i.e. $\mathbf{g}_i = \mathbf{0}$. In order to derive these internal forces two conditions are set on the overall system. The first is the compatibility condition which states that the responses on either interface are equal:

$$\mathbf{u}_b^{\mathrm{A}} - \mathbf{u}_b^{\mathrm{B}} = \mathbf{0} \quad \rightarrow \quad \mathbf{B}\mathbf{u} = \mathbf{0} \tag{5}$$

where $\mathbf{B}_{M\times N}$ is a signed Boolean matrix which denotes for the N total global DoF, the M equality conditions that need to be satisfied to impose compatibility on the interface. Note that M is now also the number of compatibility constraints placed on the system.

Next, the equilibrium condition ensures that a force equilibrium exists on the boundary. In other words, it states that the forces on one side of the interface, are equal but opposite to the forces on the other side of the interface. In LM-FBS, these forces are represented by a set of unknown Lagrange multipliers $\boldsymbol{\lambda}_{M\times 1}$. Note that it can be cast in matrix form using the same signed Boolean matrix $\mathbf{B}$.

$$\mathbf{g}_b^{\mathrm{A}} = -\mathbf{g}_b^{\mathrm{B}} = \boldsymbol{\lambda} \quad \rightarrow \quad \mathbf{B}^T\boldsymbol{\lambda} = -\mathbf{g} \tag{6}$$

Equation (6) is substituted into equation (4) which is then pre-multiplied by $\mathbf{B}$ to enforce compatibility:

$$\mathbf{B}\mathbf{u} = \mathbf{B}\mathbf{Y}\left(\mathbf{f} - \mathbf{B}^T\boldsymbol{\lambda}\right) = \mathbf{0} \tag{7}$$

This is then solved for the Lagrange multipliers (read: boundary forces), i.e. the forces needed to enforce the compatibility:

$$\boldsymbol{\lambda} = \left(\mathbf{B}\mathbf{Y}\mathbf{B}^T\right)^{-1}\mathbf{B}\mathbf{Y}\mathbf{f} \tag{8}$$

which in turn, are resubstituted into the equation of motion to derive the coupled responses using relation (6):

$$\mathbf{u} = \mathbf{Y}^{\mathrm{AB}}\mathbf{f} = \left[\mathbf{Y} - \mathbf{Y}\mathbf{B}^T\left(\mathbf{B}\mathbf{Y}\mathbf{B}^T\right)^{-1}\mathbf{B}\mathbf{Y}\right]\mathbf{f} \tag{9}$$

The coupled admittance matrix $\mathbf{Y}^{\mathrm{AB}}$ is then:

$$\mathbf{Y}^{\mathrm{AB}} = \mathbf{Y} - \mathbf{Y}\mathbf{B}^T\left(\mathbf{B}\mathbf{Y}\mathbf{B}^T\right)^{-1}\mathbf{B}\mathbf{Y} \tag{10}$$

Equation (10) is a single-line equation of LM-FBS to couple models. Note that, although only two models were coupled in the presented example, the equation holds for multiple components.

Weakening in the interface: Adding joint dynamics

Note that in the previous part the LM-FBS method is derived with strict compatibility and equilibrium between the components, and thus a rigid connection. In order to add a linear flexible joint one of two things can be done: Either the joint is added as a separate substructure into equation (10), which as explained before, is done easily. Or a joint is added as a relaxation of the compatibility condition between components A and B; this method is extensively described in [6] but will be shortly repeated here.

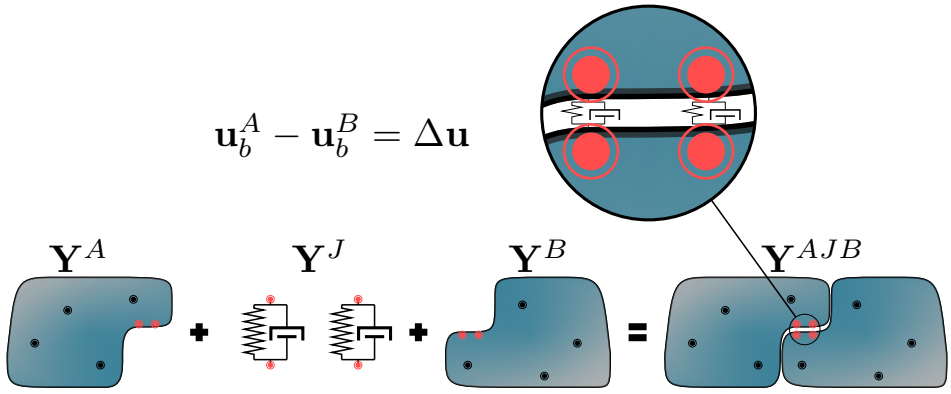

Figure 2: Component A is connected to component B via a mass-less joint represented by $\mathbf{Y}^{\mathrm{J}}$. Due to the weakened connection the compatibility condition states that $\mathbf{u}_b^{\mathrm{A}} - \mathbf{u}_b^{\mathrm{B}} = \Delta\mathbf{u}$.

In Figure 2 a flexible joint $\mathbf{Y}^{\mathrm{J}}$ is added between the interfaces of component A and B. Because of the joint, a gap can occur between the boundary DoF of the two components altering the compatibility condition from equation (5):

$$\mathbf{u}_b^{\mathrm{A}} - \mathbf{u}_b^{\mathrm{B}} = \Delta\mathbf{u} \quad \rightarrow \quad \mathbf{B}\mathbf{u} = \Delta\mathbf{u} \tag{11}$$

This gap is a response to the boundary forces $\boldsymbol{\lambda}$ which act on the joint:

$$\Delta\mathbf{u} = \mathbf{Y}^{\mathrm{J}}\boldsymbol{\lambda} \tag{12}$$

Substituting these relations into equation (4) results in:

$$\mathbf{B}\mathbf{u} = \mathbf{B}\mathbf{Y}\left(\mathbf{f} - \mathbf{B}^T\boldsymbol{\lambda}\right) = \Delta\mathbf{u} = \mathbf{Y}^{\mathrm{J}}\boldsymbol{\lambda} \tag{13}$$

which again, is solved for $\boldsymbol{\lambda}$:

$$\boldsymbol{\lambda} = \left(\mathbf{B}\mathbf{Y}\mathbf{B}^T + \mathbf{Y}^{\mathrm{J}}\right)^{-1}\mathbf{B}\mathbf{Y}\mathbf{f} \tag{14}$$

Similar to above, the weakly-coupled admittance matrix $\mathbf{Y}^{\mathrm{AJB}}$ is found to be:

$$\mathbf{Y}^{\mathrm{AJB}} = \mathbf{Y} - \mathbf{Y}\mathbf{B}^T\left(\mathbf{B}\mathbf{Y}\mathbf{B}^T + \mathbf{Y}^{\mathrm{J}}\right)^{-1}\mathbf{B}\mathbf{Y} \tag{15}$$

With equation (15) a coupled model can be created by weakening the compatibility condition. When including the joint in this manner, as compared to when including the joint as its own substructure, some extra assumptions are made:

- The joint is mass-less. This assumption is based on the fact that the equilibrium condition introduced in equation (6) remains unaltered. Therefore, the forces acting on the boundary DoF of component A and B are still equal but opposite *at all times*. Since this is no longer the case if a mass exists between the DoF (as this introduces counter-acting inertial forces), the joint is required to be mass-less. Alternatively, mass *could* be included beforehand by coupling (parts of) the joint-mass to either side of components A and B using standard LM-FBS.
- The joint model $\mathbf{Y}^{\mathrm{J}}_{M\times M}$ is constructed such that, when the boundary forces act on it, the response $\boldsymbol{\Delta}\mathbf{u}$ is the difference in response between the M boundary DoF on component A and B. There is therefore no information pertaining to the relation between DoF on any one side, i.e. it is assumed that there exists no coupling between the DoF on *one* interface which might not always be the case.

These assumptions are recognized as similar to those found in the joint identification first introduced as inverse-substructuring, explained in detail in [7, 8]. These assumptions may, on first glance, limit the scope of joints that one might be interested in. However, both assumptions are valid for lightweight and small joint (such as friction contacts, glued contacts, welds, or even bolts when applied to a large structure). In fact, the linearity assumption accompanied by frequency based methods (small displacements and rotations) may already exclude the effects of these cross-coupling terms since they are bound to be non-linear.

Decoupling the components to obtain the joint

LM-FBS can be used to decouple components from full-systems as easily as it can be used to couple components to systems. It can be shown that decoupling is as easy as adding a negative model [5]. In this case specifically, the interest is in obtaining the joint dynamics from the system $\mathbf{Y}^{\mathrm{AJB}}$, therefore decoupling is done by simply reversing equation (15). Figure 3 shows the process, which is indeed the reverse of what is shown in Figure 2. It can be shown that standard decoupling is analogous to this equation inversion.

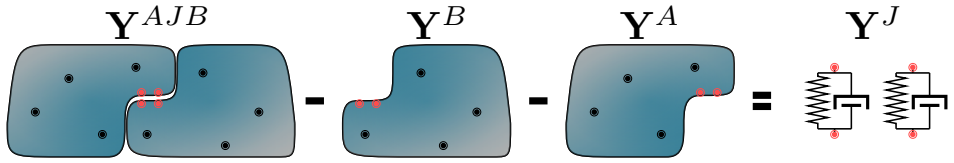

Figure 3: The components $\mathbf{Y}^{\mathrm{A}}$ and $\mathbf{Y}^{\mathrm{B}}$ are decoupled from the full model $\mathbf{Y}^{\mathrm{AJB}}$. What is left is the dynamics of the joint represented by $\mathbf{Y}^{\mathrm{J}}$.

This is done by first pre- and post-multiplying Equation (15) by $\mathbf{B}$ and $\mathbf{B}^T$ respectively and then solving it for $\mathbf{Y}^{\mathrm{J}}$ to obtain (16).

$$\mathbf{Y}^{\mathrm{J}} = -\mathbf{B}\mathbf{Y}\mathbf{B}^T - \mathbf{B}\mathbf{Y}\mathbf{B}^T \left(\mathbf{B}\boldsymbol{\Delta}\mathbf{Y}\mathbf{B}^T\right)^{-1} \mathbf{B}\mathbf{Y}\mathbf{B}^T \tag{16}$$

where $\boldsymbol{\Delta}\mathbf{Y}$ is the difference in FRF between the uncoupled and coupled model:

$$\boldsymbol{\Delta}\mathbf{Y} = \mathbf{Y}^{\mathrm{AJB}} - \mathbf{Y} \tag{17}$$

2.2 System Equivalent Model Mixing

It is shown in the previous sections that, with LM-FBS, components can be coupled with and without joints, and that a joint can be extracted from the system model. However, this still requires that the boundary DoF (c.f. the red markers in Figure 3) are known. Measuring these DoF, especially in several directions and including rotational DoF, is often practically infeasible in the *assembled state*. So what if, alternatively, one can expand a measurable DoF-set to include boundary DoF? In this section an expansion method known as SEMM will be used to expand the measured internal DoF (c.f. the black markers in Figure 3) to the required boundary DoF.

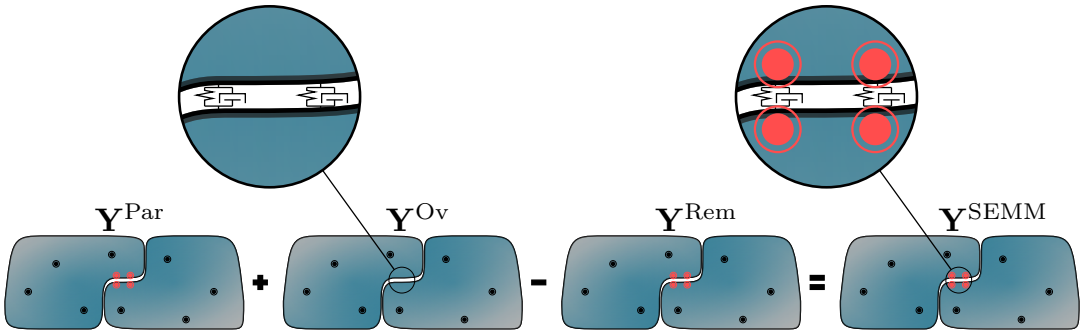

Figure 4: The parent model and overlay model are coupled. The parent model $\mathbf{Y}^{\mathrm{par}}$ contains all the DoF required but contains an erroneous joint. The overlay model $\mathbf{Y}^{\mathrm{ov}}$ is a set of measurements of the system with the correct joint, but lacks the DoF required to identify this joint. From this, the removed model –in this case a copy of the parent model– is decoupled. The resulting SEMM model $\mathbf{Y}^{\mathrm{SEMM}}$ has the *correct* joint (from the overlay model) and also has the required DoF to decouple (from the parent model).

System Equivalent Model Mixing (SEMM) is a method that uses substructuring to expand model dynamics contained in an *overlay* model $\mathbf{Y}^{\mathrm{ov}}$ onto the DoF-space of a *parent* model $\mathbf{Y}^{\mathrm{par}}$. In Figure 4 the process is drawn schematically for component AB. Let us start by stating the equation of motion for the SEMM-system which directly follows from the schematic in Figure 4.

$$\mathbf{u} = \mathbf{Y}\left(\mathbf{f} - \mathbf{g}\right), \quad \text{with} \quad \mathbf{Y} = \begin{bmatrix} \mathbf{Y}^{\mathrm{par}} & & \\ & -\mathbf{Y}^{\mathrm{rem}} & \\ & & \mathbf{Y}^{\mathrm{ov}} \end{bmatrix}, \quad \mathbf{f} = \begin{bmatrix} \mathbf{f}^{\mathrm{par}} \\ \mathbf{f}^{\mathrm{rem}} \\ \mathbf{f}^{\mathrm{ov}} \end{bmatrix}, \quad \mathbf{g} = \begin{bmatrix} \mathbf{g}^{\mathrm{par}} \\ \mathbf{g}^{\mathrm{rem}} \\ \mathbf{g}^{\mathrm{ov}} \end{bmatrix} \tag{18}$$

Here, the models $\mathbf{Y}^{\mathrm{par}}, \mathbf{Y}^{\mathrm{rem}}, \mathbf{Y}^{\mathrm{ov}}$ are the so-called parent, removed, and overlay models respectively. These are the building blocks for SEMM; they are derived below.

In order to apply the method in the joint-identification case we require:

1. FRF-based component models that contain the entire DoF-set including boundary DoF. These may be either numerical or experimental in nature (note: it may be possible to measure the boundary DoF in the *unassembled state*).
2. A set of measurements of an *assembled* full-system that observe the joint dynamics but do not have explicit boundary DoF.

Requirement one is the parent model: To compute the parent model the component models can either be left uncoupled (in block-diagonal form) or coupled with an *initial guess* joint model:

$$\mathbf{Y}^{\mathrm{par}} = \left[\mathbf{Y}^{\mathrm{AB}}_{gg}\right] = \begin{bmatrix} \mathbf{Y}^{\mathrm{AB}}_{i_A i_A} & \mathbf{Y}^{\mathrm{AB}}_{i_A i_B} & \mathbf{Y}^{\mathrm{AB}}_{i_A b_A} & \mathbf{Y}^{\mathrm{AB}}_{i_A b_B} \\ \mathbf{Y}^{\mathrm{AB}}_{i_B i_A} & \mathbf{Y}^{\mathrm{AB}}_{i_B i_B} & \mathbf{Y}^{\mathrm{AB}}_{i_B b_A} & \mathbf{Y}^{\mathrm{AB}}_{i_B b_B} \\ \mathbf{Y}^{\mathrm{AB}}_{b_A i_A} & \mathbf{Y}^{\mathrm{AB}}_{b_A i_B} & \mathbf{Y}^{\mathrm{AB}}_{b_A b_A} & \mathbf{Y}^{\mathrm{AB}}_{b_A b_B} \\ \mathbf{Y}^{\mathrm{AB}}_{b_B i_A} & \mathbf{Y}^{\mathrm{AB}}_{b_B i_B} & \mathbf{Y}^{\mathrm{AB}}_{b_B b_A} & \mathbf{Y}^{\mathrm{AB}}_{b_B b_B} \end{bmatrix} \tag{19}$$

where the (global) DoF-set g contains the boundary DoF-set b (c.f. the red markers in Figure 4) and the internal DoF-set i (c.f. the black markers in Figure 4) such that $g = \mathrm{col}\begin{bmatrix} i_A & i_B & b_A & b_B \end{bmatrix}$ are all the DoF of component AB.

Note that if the joint is in fact rigid, then due to the compatibility equation (5) the third and fourth row, and third and fourth column are redundant since DoF $b_A = b_B$. It is important that the parent model, as postulated above, contains a flexible initial guess joint such that DoF $b_A \neq b_B$ for reasons which will be explained later. Note that an uncoupled model (infinitely flexible joint) is then also permitted. In this specific case the cross-terms between the components are all zero.

Next, the full-system measurements (which observe the joint dynamics) are required. These become the so-called overlay model:

$$\mathbf{Y}^{\mathrm{ov}} = \begin{bmatrix} \mathbf{Y}^{\mathrm{AJB}}_{i_A i_A} & \mathbf{Y}^{\mathrm{AJB}}_{i_A i_B} \\ \mathbf{Y}^{\mathrm{AJB}}_{i_B i_A} & \mathbf{Y}^{\mathrm{AJB}}_{i_B i_B} \end{bmatrix} \tag{20}$$

As stated before, the measurements can only be done for the internal DoF i_A, i_B.

Finally, SEMM requires the *removed model* which is none other than (a reduced form of) the parent model (c.f. Figure 4). One can choose to formulate the removed model as the parent model itself, or as a reduced form of of the parent model which contain only the internal DoF i_A, i_B [2]. An explanation on the differences is omitted in this paper, but is given in [4]. In this application, it is chosen for the removed and parent model to be the same size and thus the same:

$$\mathbf{Y}^{\text{rem}} = \mathbf{Y}^{\text{par}} \tag{21}$$

To solve (18) the compatibility and equilibrium constraints are applied as in LM-FBS. Compatibility requires:

$$\mathbf{u}_g^{\text{par}} - \mathbf{u}_g^{\text{rem}} = \mathbf{0} \tag{22a}$$
$$\mathbf{u}_i^{\text{rem}} - \mathbf{u}_i^{\text{ov}} = \mathbf{0} \tag{22b}$$

The equilibrium condition reads:

$$\mathbf{g}_b^{\text{par}} + \mathbf{g}_b^{\text{rem}} = \mathbf{0} \tag{23a}$$
$$\mathbf{g}_i^{\text{par}} + \mathbf{g}_i^{\text{rem}} + \mathbf{g}_i^{\text{ov}} = \mathbf{0} \tag{23b}$$

Like before, the compatibility and equilibrium condition can be written in matrix-notation with the signed Boolean Matrix $\mathbf{B}$:

$$\text{Compatibility} : \mathbf{Bu} = \mathbf{0}, \quad \text{Equilibrium} : \mathbf{g} = \mathbf{B}^T\boldsymbol{\lambda}, \quad \text{with} \quad \mathbf{B} = \begin{array}{c} \begin{matrix} \mathbf{u}_i^{\text{par}} & \mathbf{u}_b^{\text{par}} & \mathbf{u}_i^{\text{rem}} & \mathbf{u}_b^{\text{rem}} & \mathbf{u}_i^{\text{ov}} \end{matrix} \\ \left[\begin{array}{ccc|c|c} \mathbf{I} & \mathbf{0} & -\mathbf{I} & \mathbf{0} & \mathbf{0} \\ \mathbf{0} & \mathbf{I} & \mathbf{0} & -\mathbf{I} & \mathbf{0} \\ \mathbf{0} & \mathbf{0} & \mathbf{I} & \mathbf{0} & -\mathbf{I} \end{array}\right] \end{array}$$

The formulation exactly follows the LM-FBS notation described above, thus it is solved with equation (10). It can be shown that from this solution the single-line equation of SEMM can be obtained. The derivation is omitted in this paper, but can also be found in [4]:

$$\mathbf{Y}^{\text{SEMM}} = \mathbf{Y}_{gg}^{\text{par}} - \mathbf{Y}_{gg}^{\text{par}} \left(\mathbf{Y}_{ig}^{\text{par}}\right)^{+} \left(\mathbf{Y}_{ii}^{\text{par}} - \mathbf{Y}_{ii}^{\text{ov}}\right) \left(\mathbf{Y}_{gi}^{\text{par}}\right)^{+} \mathbf{Y}_{gg}^{\text{par}} \tag{24}$$

Here we made use of the relation (21) to substitute the terms of the removed model.

The SEMM model now contains the dynamics from the overlay model while including the boundary DoF's required to extract the joint model with equation (16).

When expanding a DoF-set, new information is extrapolated based on the information contained in the measurements of the overlay model. Unfortunately, such an extrapolation is generally erroneous. Consequently, any joint model extracted from the expanded SEMM model is also erroneous (although presumably less so than in the original parent model).

If one assumes that the overlay model contains the correct dynamics, then the only error made is this extrapolation error. It comes solely from the parent model's manifold (i.e. its modal content) differing from that of the *correct* overlay model. In other words, even though the SEMM method will alter the dynamics of the parent model to fit that of the overlay model, it can only do so based on the allowable modal directions of said parent model. This is because any deflection shape created by the parent model must still be a linear combination of its modeshapes.

[2] Note that reduction in admittance space is done by simply removing the DoF from the matrix.

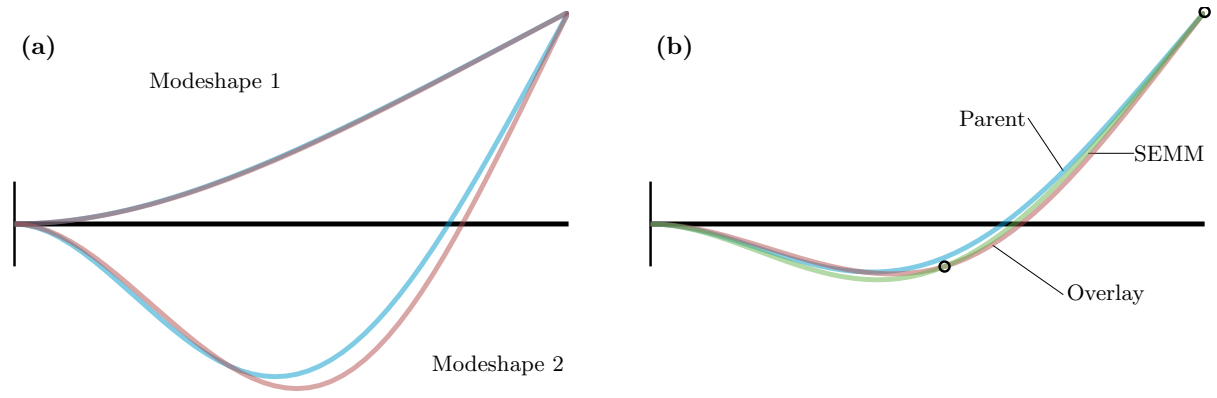

Figure 5: (a): A clamped beam with two modeshapes. The first modeshape is equal for both the parent and overlay model. The second is different for the parent (blue) and overlay model (red). (b): The *normalized* deflection shapes of each model for a given actuation. The SEMM model (green) is equal to the overlay model on the control points (black circles) but differs at the other locations since its end result must be a linear combination of the parent modeshapes given in (a). This off-set is the expansion error ε

Figure 5 illustrates this simple fact with a short example of a clamped-free beam which – for simplicity – has only the first two modes. These are depicted in (a). The first mode-shape is relatively the same for both parent (red) and overlay (blue) model, yet the second differs. The *normalized* deflection shapes of the parent (red), overlay (blue) and resulting SEMM (green) model for a given actuation are illustrated in (b). When looking at the SEMM model, even though the shared DoF match as per design, the internal DoF cannot since the required deflection shape is not a linear combination of the parent mode-shapes.

This is also the reason that no rigid connection should be used to couple the component models $\mathbf{Y}^{\mathrm{A}}$ and $\mathbf{Y}^{\mathrm{B}}$ to create the parent model $\mathbf{Y}^{\mathrm{AB}}$. Since, if that were the case, the compatibility condition would ensure that $b_A = b_B$ in the entire modal space; i.e. there exist no modal direction in which a gap –and thus joint dynamics– exists. Since the parent model can only adapt to the overlay model in the modal directions, forming a gap is a non-controllable direction. Consequently, the gap is never created and thus no joint would be able to be identified!

In the single-line equation (24) one can observe that any changes made to the parent model (including expansion error) is made in the second term of this equation. This second term is proportional to the difference between the parent and overlay model. The error ε of the SEMM expansion is therefore –in some form– proportional to the difference in overlay and parent model:

$$\varepsilon \propto \left\| \mathbf{Y}_{ii}^{\mathrm{par}} - \mathbf{Y}_{ii}^{\mathrm{ov}} \right\| \tag{25}$$

Also note that in the trivial solution when the overlay model and parent model are equal, there is no *observable* error in the SEMM model since $\mathbf{Y}_{ii}^{\mathrm{SEMM}} = \mathbf{Y}_{ii}^{\mathrm{ov}} = \mathbf{Y}_{ii}^{\mathrm{par}}$. The term observable error is used here to accentuate that an error might still exist on the DoF which do not explicitly exist for the overlay model, and thus cannot be observed. Note that the reason enough internal DoF must be taken into account is to ensure the observability of this error and by extension the joint dynamics. If this is the case, one can derive from equation (25) that the parent and overlay model must converge to minimise the expansion error.

2.3 The Optimisation Scheme

Unfortunately the joint identified from the SEMM model is not perfect due to the expansion error discussed in the previous section. Now let us assume that the *only* difference between the parent and overlay model is due to the joint dynamics. If the joint model extracted from the SEMM model is closer (i.e. converged) to the joint implicit in the measurements, then surely this joint can be used to create a parent model which further resembles the overlay model. Due to this convergence, the expansion error of equation (25) is decreased which would result in a better identification of the joint. Repeating this, the process would converge to the identification of the true joint.

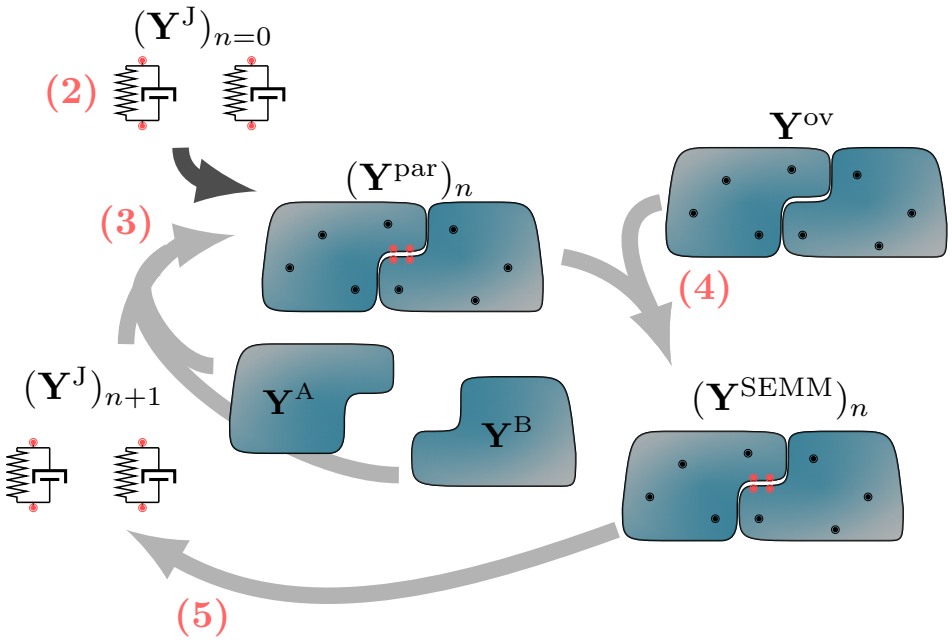

Figure 6: The joint optimisation process. The initial joint (2) is used to create a parent model (3). The parent model is coupled to the overlay model in the SEMM process (4). From the new SEMM model a new joint is identified (5). This new joint is used to create a new parent model (3). The process is then repeated until parent and overlay model converge.

Following this conjecture, an iterative process can be described, its schematic is illustrated in Figure 6:

1. Measurements are performed on the assembled system, these measurements have implicit information of the joint, but lack boundary DoF measurements: this becomes the overlay model $\mathbf{Y}^{\mathrm{ov}}$.
2. An *initial guess* for the joint is constructed: $\mathbf{Y}^{J}_{n=0}$.
3. This joint is used to couple the component models A and B: this becomes the n^{th} parent model $(\mathbf{Y}^{\mathrm{par}})_n$.
4. SEMM is performed with the parent and overlay model in order to obtain the SEMM model $\mathbf{Y}^{\mathrm{SEMM}}_{n}$.
5. Decoupling using Equation (16) is performed to extract a new joint model from the SEMM model: $\mathbf{Y}^{J}_{n+1}$.
6. Steps 3 - 5 are repeated until the difference between parent and overlay model –and thus the expansion error of equation (25)– is minimised.

There are some things that must be considered when implementing this scheme. In reality there are more error sources than just the SEMM expansion error (one can think of measurement errors, incorrect component models, incorrect DoF locations, etc.) and these errors will pollute the optimisation such that a true optimum may never be found in practice. Nevertheless, some techniques may be implemented to clean up the results such that a good estimation can still be achieved:

- If some notion of the joint geometry is known (such as there being no cross-couplings) a fitting can be done to acquire some (physical) properties of the joint. Knowing that the joint properties are –to some extent– frequency independent, one could implement this method at frequencies where the joint dynamics are more prevalent compared to the system dynamics. At these frequencies the observability of the joint is higher, resulting in a higher signal to noise ratio when decoupling. Such principles have been used successfully in the past. [3].
- It may be that the method jumps between solutions, resulting in local optima. One can choose to average out past results such that the new joint $(\mathbf{Y}^{\mathrm{J}})_{n+1}$ is a mix between past results: $(\mathbf{Y}^{\mathrm{J}})_{n+1}$, $(\mathbf{Y}^{\mathrm{J}})_{n}$, $(\mathbf{Y}^{\mathrm{J}})_{n-1}$. This is in effect a relaxation scheme and can also be interpreted as analogous to implementing numerical damping in e.g. Newmark methods.

- Since only the joint is of importance, the quality of the component models is secondary. Yet, since this method does not discriminate between error in the joint model and error in the sub-components, any discrepancy between the sub-component models in the parent versus the overlay model is going to pollute the result. It might be important to ensure that, at the very least, the component models $\mathbf{Y}^{\mathrm{A}}$ and $\mathbf{Y}^{\mathrm{B}}$ are equal in both the parent and (implicit) overlay model. If the parent model is measured in the same manner (but disassembled) as the overlay model, then any measurement bias is also shared by both the parent and overlay model which will reduce this type of error.

3 A NUMERICAL STUDY

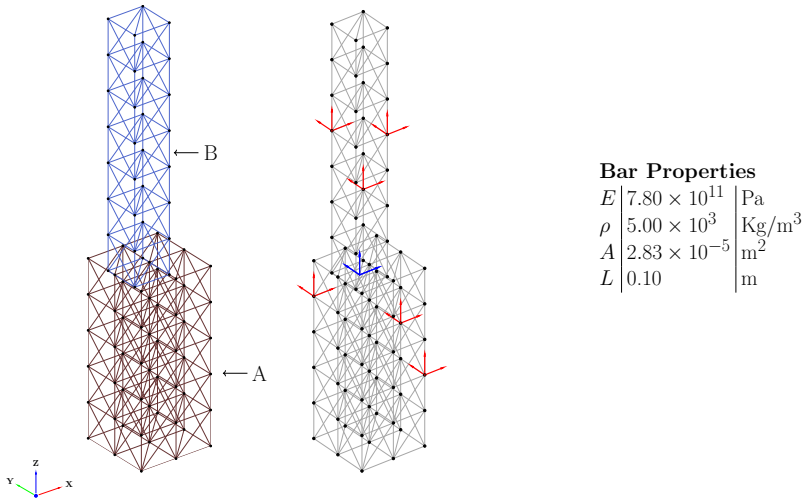

Figure 7: The truss structure used in this test-case. On the left the two parts of the assembly are colour-coded. The bottom part (Structure A) is fixed at the bottom. Structure B is attached to structure A via a joint in 6-DoF. On the left the assembly AB is shown as a whole. The blue node is the location of the joint. The red nodes are the measurement locations, i.e. the internal DoF used in the SEMM-optimisation scheme. It is important to note that the structures are only connected via this 6-DoF connection point. The structure B is placed on A in such a way that symmetry is avoided.

A small numerical case is presented as a proof of concept. For this case the connection of two bar-truss structures shown in Figure 7 is investigated. The truss structures are connected via a 6-DoF joint: 3 translational and 3 rotational DoF on a node in the centre (c.f. the blue node on the right side of Figure 7) which acts as the interface. The centre-node is created by means of a RBE-3 spider element from the nodes at each structure's end. Note that the measurement locations (c.f. the red nodes in the right image of Figure 7) are spread so that the joint dynamics are observable. Also note that none are on the interface area or inaccessible locations.

Table 1: The parameters (stiffness k and damping c coefficients) of the joints tested. The parameters of the *initial-guess* joint used in the first iteration of the parent model is also provided. These parameters are used in both test-cases.

	Strong Joint		Weak Joint		Initial Guess	
DoF	k	c	k	c	k	c
x	1×10^8	100	1×10^4	100	1×10^2	0
y	1×10^8	100	1×10^4	100	1×10^2	0
z	1×10^{10}	1	1×10^6	1	1×10^2	0
θ_x	1×10^{10}	10	1×10^6	10	1×10^2	0
θ_y	1×10^{10}	10	1×10^6	10	1×10^2	0
θ_z	1×10^8	100	1×10^3	100	1×10^2	0

Two joints are investigated: a *weak* joint and a *strong* joint. The *strong* joint's influence on the structure is noticeable but

minimal. The *weak* joint is chosen such that it almost fully determines the assembly's dynamics. Only DoF-to-DoF damping and stiffness is investigated: no cross-coupling between DoF exist in the tested joints. Furthermore, the damping values are kept equal for both. The parameters of the joints are given in Table 1.

The optimisation scheme is run for several iterations; 20, 100 and 200 iterations are run which require approximately $2.5, 12.5, 25$ seconds computation time respectively. In Figure 8 the driving-point frequency response functions of the system $\mathbf{Y}^{\mathrm{AB}}$ for the boundary DoF θ_z are given; the graphs represent the results after the pre-determined number of iterations for both the case of the weak (left) and strong (right) joint. The reference FRF and the FRF of the rigidly connected $\mathbf{Y}^{\mathrm{AB}}$ are also provided as a comparison.

The FRF follow the reference throughout a large part of the frequency band. An interesting error occurs at or near the resonance frequencies of the *would-be* rigidly fixed system $\mathbf{Y}^{\mathrm{AB}}$. The results show that the optimising scheme cannot identify the joint near these frequencies.

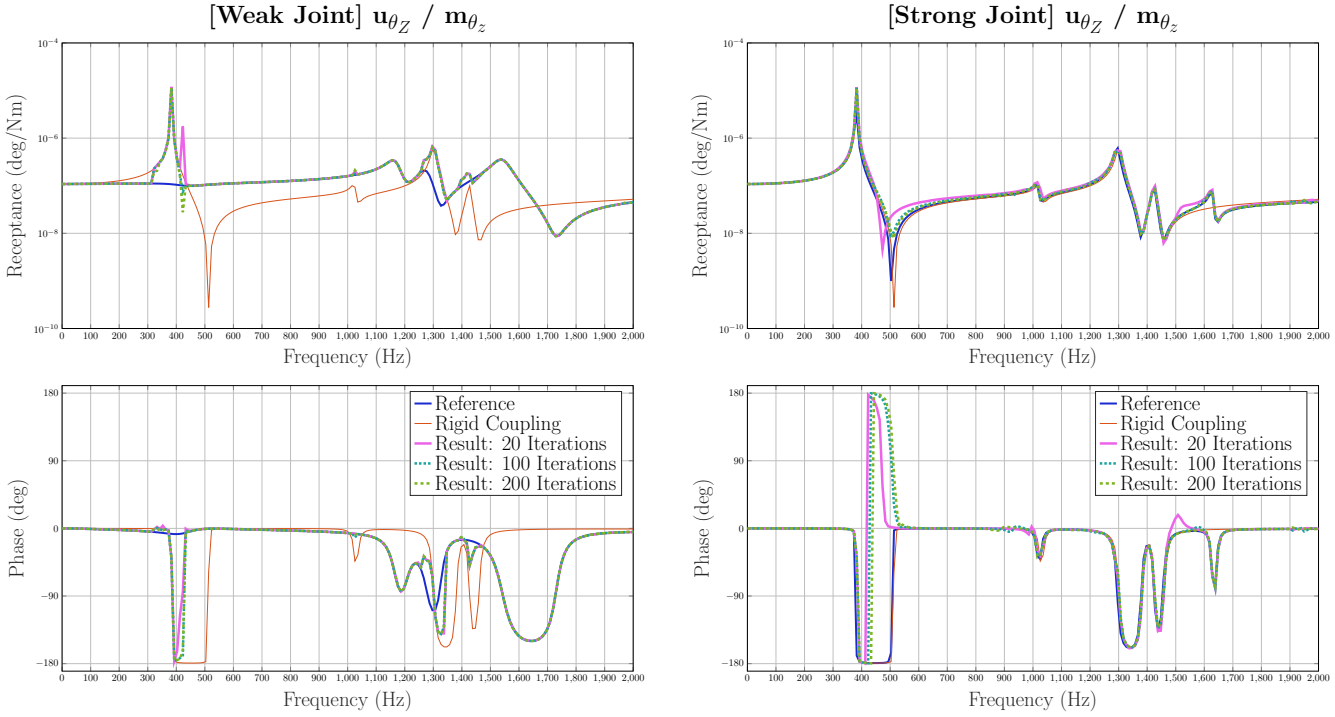

Figure 8: The driving-point FRF on DoF θ_z. The FRF of the *weak* joint are given on the left and the FRF of the *strong* joint are given on the right. In both cases – and even after only a few iterations – the FRF seem to follow the reference; the exception being near the resonance frequencies of the rigid coupling. This results in spurious peaks near those frequencies.

Next, the linear joint parameters can be identified from the FRF of the joint $\mathbf{Y}^{\mathrm{J}}$. In order to do this, a frequency band is chosen such that it contains no resonance frequencies of the rigidly coupled $\mathbf{Y}^{\mathrm{AB}}$ in order to ensure that the previously observed error does not pollute these results. For this example the frequency band from $450\,\mathrm{Hz}$ to $850\,\mathrm{Hz}$ is chosen. The joint parameters are extracted by means of a curve-fit of the driving-point FRF of $\mathbf{Z}^{\mathrm{J}}_n = (\mathbf{Y}^{\mathrm{J}}_n)^{-1}$

It is important to remember that this fitting does not influence the optimisation since the optimisation uses the raw model $\mathbf{Y}^{\mathrm{J}}_n$ for each subsequent step. In Table 2 the results of the fitting for $n = 20, 100$ and 200 are given. It is immediately apparent that these joint properties are non-physical! Most of the stiffness values are –with the exception of k_y– negative which indicates an active joint. However, it is important to note two things: first, even though the values are off, the FRF in Figure 8 follow the reference FRF in amplitude and phase. Second, as the number of iterations increase, the joint parameters remain relatively the same. This indicates that the resulting joint parameters are approaching a (non-physical) local optimum, i.e. it indicates that multiple solutions exist that are indistinguishable from the chosen set of observation DoF.

Table 2: The fitted parameters of the *strong* joint. Δ is the difference between the value and its reference given in orders of magnitude. The results for both the stiffness k and damping values c are off by up to a few orders.

Strong Joint

20 Iterations		100 Iterations		200 Iterations	
k	Δ	k	Δ	k	Δ
-4.57×10^7	-0.340	-3.19×10^7	-0.496	-3.28×10^7	-0.485
7.25×10^6	1.140	3.13×10^7	0.505	4.56×10^7	0.341
-5.28×10^8	-1.277	-4.73×10^8	-1.325	-4.31×10^8	-1.366
-1.22×10^6	-3.915	-1.75×10^6	-3.756	-3.12×10^6	-3.505
-2.76×10^7	-2.558	-3.08×10^7	-2.511	-3.11×10^7	-2.508
-1.05×10^8	-0.020	-9.88×10^7	-0.005	-9.58×10^7	-0.019
c	Δ	c	Δ	c	Δ
1079.7	1.033	1571.60	1.196	2265.5	1.355
60.9	0.215	446.98	0.650	710.1	0.851
4053.8	3.608	4053.99	3.608	4100.8	3.613
11.7	0.067	30.68	0.487	-15.8	-0.198
163.4	1.213	106.00	1.025	11.6	0.064
685.8	0.836	491.74	0.692	377.1	0.576

Similarly the joint parameters of the weak joint can be identified. The same frequency band is used. Note that already after a few iterations the real joint parameters are found accurately for all DoF with the exception of the DoF θ_x. This may indicate that the observability of this DoF is poor. Nevertheless, as the iterations increase the optimisation converges to the true values.

Table 3: The fitted parameters of the *weak* joint. Δ is the difference between the value and its reference given in orders of magnitude. The results for both the stiffness k and damping values c are all very close to the true values. The exception is the DoF θ_x.

Weak Joint

20 Iterations		100 Iterations		200 Iterations	
k	Δ	k	Δ	k	Δ
9.91×10^3	0.004	9.88×10^3	0.005	9.84×10^3	0.007
1.00×10^4	0.002	9.93×10^3	0.003	9.91×10^3	0.004
9.97×10^5	0.001	9.99×10^5	0.000	9.99×10^5	0.000
1.71×10^4	1.768	6.19×10^4	1.208	1.03×10^5	0.985
1.00×10^6	0.001	9.95×10^5	0.002	9.93×10^5	0.003
-7.98×10^2	-0.098	7.15×10^2	0.146	4.37×10^2	0.360
c	Δ	c	Δ	c	Δ
100.0	0.000	100.0	0.000	100.0	0.000
100.1	0.000	100.0	0.000	100.0	0.000
0.7	0.150	1.0	0.002	1.0	0.001
0.2	1.619	0.6	1.234	0.9	1.049
10.1	0.005	9.9	0.006	9.8	0.008
99.7	0.001	100.0	0.000	100.0	0.000

4 DISCUSSION

The FRF of Figure 8 show that the joint identification results follow the reference FRF for frequencies other than at or near the resonance frequencies of the rigidly connected system $\mathbf{Y}^{\mathrm{AB}}$. Furthermore, the extraction of joint parameters show that better results are obtained for the *weak* joint. This suggests that the joint identification can only be done when the joint dynamics are sufficiently observable.

Some additional thoughts are provided to contextualize the results:

- The optimisation scheme performs poorly at and near the resonance frequencies of the rigidly connected system $\mathbf{Y}^{\mathrm{AB}}$. This results in spurious peaks; at these frequencies the optimisation is forced towards the rigid connection. As explained in section 2.2: once the rigid connection is formed, the gap between the respective boundary DoF of structures A and B is closed. Remember that once closed, the gap cannot be opened since then the optimisation directions (the modal directions of the parent model) also contain no gap. A rigid connection can therefore be regarded as an –unwanted– local optimum.
- The structure used in this test-case is chosen for its simplicity. However, it might be that this case is too simple. The truss elements are created with bar elements [3] which hinders observability since it is hard to pinpoint the connectivity between the boundary and chosen internal DoF. For example, the results in Table 3 show that all the joint parameters are found accurately after only a few iterations, yet the stiffness and damping values of DoF θ_x were not. This indicates a lack of observability on this DoF which is curious considering the chosen locations of the internal DoF.

5 CONCLUSION

A SEMM-based method can be used to identify a joint without directly measuring the interface of an assembled system. The joint must be observed with the measurements performed and included in the overlay model. However, if this is the case any number of boundary DoF can be investigated within a single measurement campaign. That is to say: as long as the observability condition is met one could identify a joint with the same overlay model coupled to a parent model with any desired translational or rotational boundary DoF.

A numerical proof of concept is provided and for specific cases the joint is accurately identified but many envisioned error sources have been omitted. The additional error sources mentioned in section 2.3 should first be investigated before any practical applications can realistically be performed. Nevertheless, the methodology is promising since it suddenly allows users to do a preliminary (read: linear) investigation of complex joints, unlimited by the inaccessibility of common interfaces.

ACKNOWLEDGEMENTS

The project has received funding from the European Union's Horizon 2020 research and innovation programme under the Marie Sklodowska-Curie grant agreement No. 721865.

[3] Many connections are therefore implicit, e.g. bending stiffness is created by the geometry of the truss, rather than in the element itself

REFERENCES

[1] D. J. Ewins, D. Nowell, and E. Petrov, "The Importance of Joints on the Dynamics of Gas Turbine Structures," in *Report on the SNL/NSF International Workshop on Joint Mechanics* (D. J. Segalman, L. A. Bergman, and D. J. Ewins, eds.), (Arlington, Virginia), pp. 23–32, Sandia National Laboratories, 2006.

[2] O. Özşahin, A. Ertürk, H. N. Özgüven, and E. Budak, "A closed-form approach for identification of dynamical contact parameters in spindle-holder-tool assemblies," *International Journal of Machine Tools and Manufacture*, vol. 49, no. 1, pp. 25–35, 2009.

[3] Ş. Tol and H. N. Özgüven, "Dynamic characterization of bolted joints using FRF decoupling and optimization," *Mechanical Systems and Signal Processing*, vol. 54, pp. 124–138, 2015.

[4] S. W. B. Klaassen, M. V. van der Seijs, and D. de Klerk, "System Equivalent Model Mixing," *Mechanical Systems and Signal Processing*, vol. 105, pp. 90–112, 2018.

[5] D. de Klerk, D. J. Rixen, and J. de Jong, "The Frequency Based Substructuring (FBS) Method Reformulated According to the Dual Domain Decomposition Method," in *IMAC-XXIV A conference & exposition on structural dynamics*, 2006.

[6] S. N. Voormeeren, P. L. C. V. D. Valk, and D. J. Rixen, "Practical Aspects of Dynamic Substructuring in Wind Turbine Engineering," in *IMAC-XXVIII A conference & exposition on structural dynamics A conference & exposition on structural dynamics*, (Jacksonville, Florida), Springe, 2010.

[7] J. W. R. Meggitt and A. T. Moorhouse, "the in-Situ Decoupling of Resiliently Coupled Sub-," in *24th International congress on sound and vibration*, no. July, (London), pp. 1–8, 2017.

[8] M. Haeussler, S. W. B. Klaassen, and D. J. Rixen, "Comparison of Substructuring based techniques for dynamic property identification of rubber isolators," in *ISMA 2018 - International Conference on Noise and Vibration Engineering*, no. August, (Leuven), p. 1, 2018.